Materials Science-Poland, 39(3), 2021, pp. 395-409
http://www.materialsscience.pwr.wroc.pl/
DOI: 10.2478/msp-2021-0032

Microstructure, tribological performances, and wear mechanisms of laser-cladded TiC-reinforced NiMo coatings under grease-lubrication condition

Zhu Weixin[1], Kong Dejun[1,*]

[1]School of Mechanical Engineering, Changzhou University, Changzhou 213164, P.R. China

NiMo-5%TiC, NiMo-15%TiC, and NiMo-25%TiC coatings were prepared on GCr15 steel by laser cladding (LC). The microstructure and the phases of the obtained coatings were analyzed using ultra-depth-of-field microscopy (UDFM) and X-ray diffraction (XRD), respectively. A ball-on-disk wear test was used to analyze the friction-wear performance of the substrate and the NiMo-TiC coatings under grease-lubrication condition. The results show that the grain shape of NiMo-TiC coatings is dendritic. The wear resistance of NiMo-TiC coatings is improved by the addition of TiC, and the depths of the worn tracks on the substrate and on the NiMo-5%TiC, NiMo-15%TiC, and NiMo-25%TiC coatings are 4.183 μm, 2.164 μm, 1.882 μm, and 1.246 μm, respectively, and the corresponding wear rates are 72.25 $\mu m^3/s/N$, 32.00 $\mu m^3/s/N$, 18.10 $\mu m^3/s/N$, and 7.99 $\mu m^3/s/N$, respectively; this shows that the NiMo-25%TiC coating has the highest wear resistance among the three kinds of coatings. The wear mechanism of NiMo-TiC coatings is abrasive wear, and the addition of TiC plays a role in resisting wear during the friction process.

Keywords: *laser cladding, NiMo coating, TiC-reinforced phase, wear rate, wear mechanism*

1. Introduction

Rolling bearings occupy an important position in machinery industry, in which GCr15 steel is one of the main steel grades due to its distinguished wear resistance. However, GCr15 steel still cannot meet the high requirements of wear resistance in the field of bearings [1], which is particularly needed to improve its hardness and lubrication performance [2, 3]. Previous researches have indicated that the coating technology may effectively increase the surface performance and extend the service life of bearings [4].

At present, there are many studies on Ni-based alloy coatings, which are applied to improve the friction-wear performance of bearings. Zikin et al. [4] revealed that the TiC-NiMo-reinforced hardfacings exhibited higher wear resistance compared with the WC/W_2C-reinforced coatings. Tan et al. [5] studied the tribological performance and wear model of TiC-reinforced Ni-based alloy coatings. Téllez-Villaseñor et al. [6] reported the effects of load and sliding velocity on the wear behavior of infiltrated TiC/Cu-Ni composites. Further, Wang et al. [7] investigated the in-situ TiC particle-reinforced Ni-based composite by selective laser melting and showed that it had excellent processability and mechanical properties.

There are many surface modifications such as carburizing, nitriding, and laser cladding (LC). Especially, LC is a new type of surface-strengthening method, in which metal powders are melted using high laser energy and solidified to form the coating on the substrate. The fabricated coatings with fine microstructure, low dilution rate, and small heat-affected zone [8, 9] may combine closely with the substrate, which can form a metallurgical bonding at the coating interfaces [8, 9]. Usually, LC is performed on metal composite coatings composed of Ni or Fe, which are supplemented by the strengthening phases, and then achieves the purpose of hardening the surface of the substrate [4, 10].

In order to further improve the wear performance of the NiMo coating, addition of ceramic carbides has become a developing trend. Compared

* E-mail: kong-dejun@163.com

with other cemented carbides, TiC with low coefficient of friction (COF) and high oxidation resistance [11, 12] can be added to the NiMo coating, which improves the hardness and wear resistance of the coating [13]. However, there are few related reports of TiC-reinforced NiMo coatings, which hinders its application in the field of bearings.

In this study, LC was used to prepare NiMo coatings with TiC as the reinforcing phase on GCr15 steel. The aim was to investigate the effect of TiC addition on the tribological performance of the NiMo coating. Moreover, the wear mechanism was also analyzed, which formed the basis for a new modification method for the bearings.

2. Experimental

2.1. Sample preparations

The substrate was commercial GCr15 bearing steel, which was ground with SiC abrasive papers of 400-1,000# in water and then cleaned with alcohol for the fabrication of the coating. The nominal chemical composition of NiMo powder was Ni: 80 and Mo: 20 (mass %). The NiMo-5%TiC, NiMo-15%TiC, and NiMo-25%TiC powders were used as the LC materials, which were mixed on a planetary ball miller. The technical parameters were shown as follows: ball and powder ratio of 10:1; speed: 500 rev/min; and time: 60 min.

The LC test was carried out on a ZKSX-2000 W type fiber-coupled laser processing system with lateral powder feeding, and the coating was covered by the multilayer overlapping method. Through many pre-experiments, the technical parameters were determined according to the bonding state between the coating and the substrate as follows: laser power: 1,700 W; laser spot diameter: 4 mm; laser power density: 135.28 W/mm^2; scanning speed: 3 mm/s; power feeding speed: 10 mL/min; and overlap ratio: 50%.

2.2. Characterization methods

After the LC test, the sample for tribological tests was lapped to a mirror finish on a metallographic polishing machine. The surfaces and cross-sections of the obtained coatings were polished on a metallographic polishing machine, and their microstructure and phases of the obtained coatings were analyzed using ultra-depth-of-field microscopy (UDFM; VHX-700FC microscope) and X-ray diffraction (XRD; D/max 2500PC diffract meter), respectively. The metallographic image analysis software Image-J with the threshold technology was used to measure the surface porosity. A HXD-1000 micro-hardness tester was used to measure the hardness, and the test parameters were load of 5 N and retention time of 10 s.

2.3. Friction-wear tests

The wear ways of bearings were divided into scrolling and sliding [14]. In this case, the friction-wear test was carried out using a CFT-I type friction and wear tester with the sliding friction method, and 30mL of lubricating grease was used to simulate the working state of bearings, as shown in Figure 1, in which the working mode adopted a crank-slider mechanism. The coatings were placed in the container, which were fixed together with the slider. The tribo-pair was imposed on the coating surfaces under normal load. The test parameters were shown as follows: tribo-pair of Si_3N_4 ball; diameter of 3 mm; load of 8 N; speed of 400 rev/min; reciprocating length of 4 mm; and duration time of 90 min. The above tests were repeated five times for each coating, and the data were averaged as the experimental results.

In this case, the wear rate was

$$\phi = \frac{v}{I} \tag{1}$$

where V was the wear volume (cubic micrometer; μm^3); and I was the impulse (newton-second; N·s).

The wear volume in Eq. (1) was

$$V = S \times L \tag{2}$$

where S was the cross-sectional area of the worn track (square micrometer; μm^2); and L was the total length of the slide (micrometer; μm).

And the impulse in Eq. (1) was

$$I = T \times F \tag{3}$$

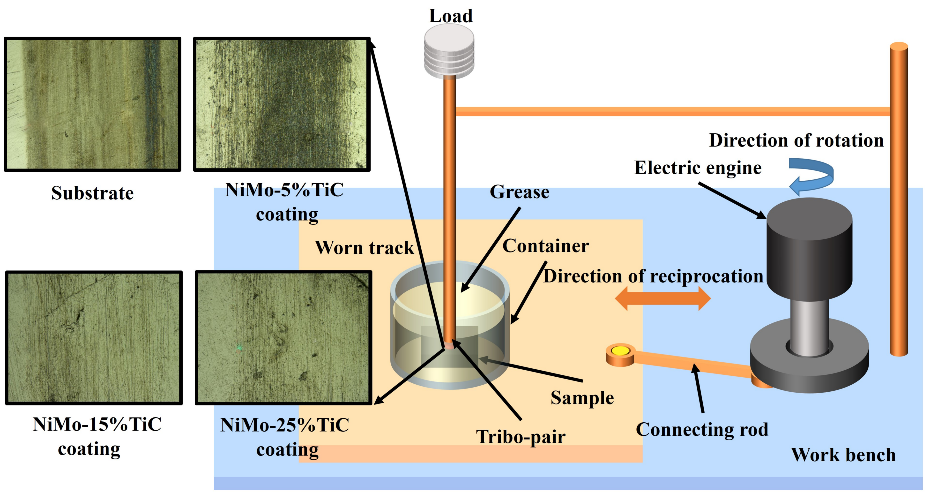

Fig. 1. Sketch of friction-wear test for NiMo-TiC coatings.

where T was the friction time (second; s); and F was the normal load (newton; N).

After the wear test, the profiles, morphologies, and chemical elements of the worn tracks on the TiC-reinforced NiMo coatings were analyzed by using UDFM, scanning electron microscopy (SEM), and energy dispersive X-ray spectrometry (EDS), respectively. The wear models were established to examine the effect of TiC on the friction-wear performance of NiMo coatings.

3. Analysis and discussion

3.1. Microstructure and porosity of coating surfaces

Figure 2(a) shows the microstructure of NiMo-5%TiC coating with the rod-shaped and petal-shaped TiC, and the grain type of the coating was dendrite. The shapes of the crystal grains were mainly determined by the ratio (N/G) of the nucleation rate (N) and the growth rate (G) [15], which were formed under a fast cooling rate at high temperature [16]. In the LC process, the coating crystals were rapidly nucleated, which formed the dendrites on the NiMo-TiC coatings [17]. Besides, petal-shaped and rod-shaped particles were also found on the coating surface. Figure 2(b) shows the microstructure of the NiMo-15%TiC coating with the rod-shaped and petal-shaped TiC particles [18]. Compared with the NiMo-5%TiC coating, the fine particles were significantly reduced due to the increase in TiC mass fraction. Figure 2(c) shows the microstructure of the NiMo-25% coating. The increase in TiC mass fraction changed the fine particles to petal-shaped particles [19]. There were also some bulk-shaped grains, which were formed by the aggregation of the undecomposed TiC [20]. The nucleation rate of the coating increased due to the increase of TiC mass fraction, which inhibited the formation of rod-shaped particles [21].

Porosity is an important index of LCed coatings. In this study, Image-J was used to calculate the coating porosity. The porosity of the NiMo-5%TiC, NiMo-15%TiC, and NiMo-25%TiC coatings in Figure 1 was 1.53%, 0.9%, and 0.8%, respectively, as shown in Figure 3, in which the black area and white dots were the coating and pores, respectively. The coating porosity decreased as the mass fraction of TiC increased. And it can be suggested that the TiC-reinforced phase reduced the coating porosity, and the porosity of NiMo-25%TiC coating was the lowest among the three kinds of coatings.

Generally, the coating's hardness decreased due to high porosity [22], which was an important index to estimate the wear resistance of coating. As a re-

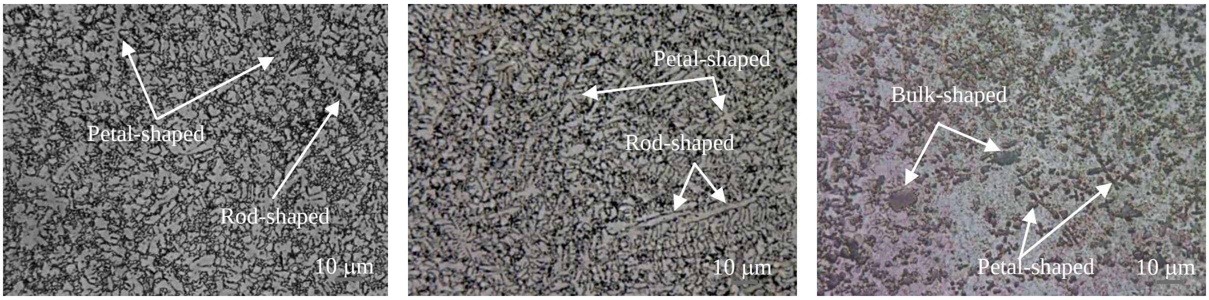

(a) (b) (c)

Fig. 2. Microstructure of NiMo-TiC coating with different TiC mass fractions: **(a)** NiMo-5%TiC coating; **(b)** NiMo-15%TiC coating; **(c)** NiMo-25%TiC coating.

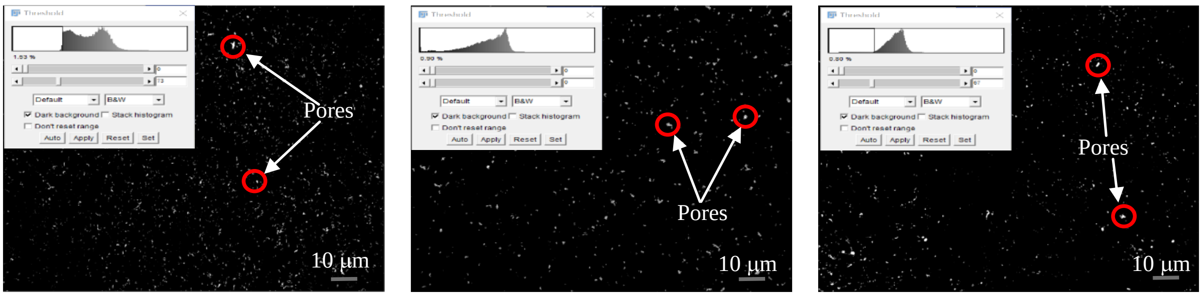

(a) (b) (c)

Fig. 3. Binary images of NiMo-TiC coatings with different TiC mass fractions: **(a)** NiMo-5%TiC coating; **(b)** NiMo-15%TiC coating; **(c)** NiMo-25%TiC coating.

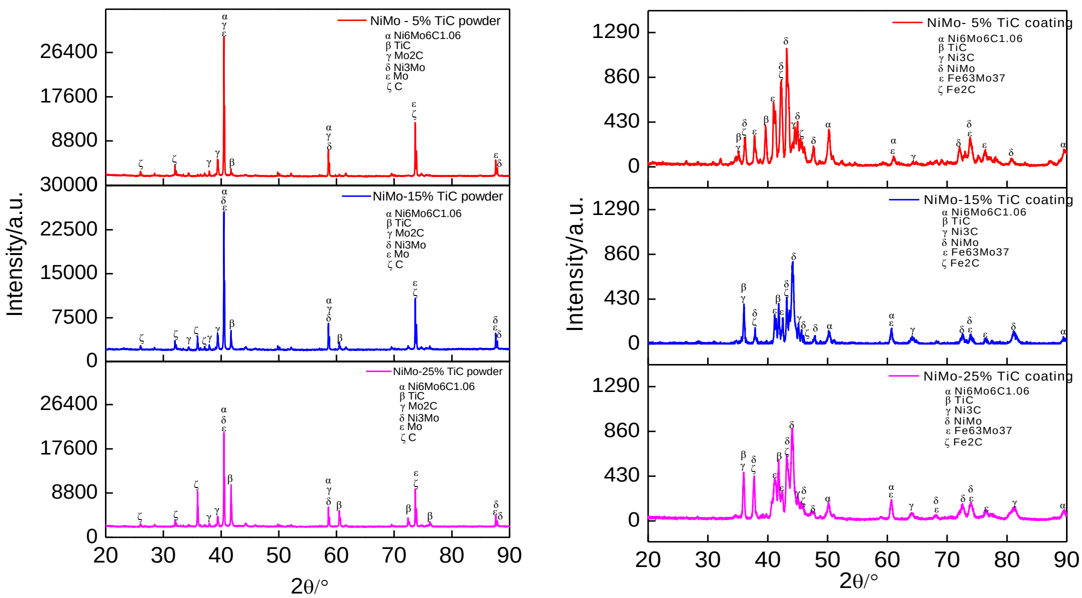

(a) (b)

Fig. 4. XRD analysis of NiMo-TiC mixed powders and coatings with different TiC mass fractions: **(a)** NiMo-TiC mixed powders; **(b)** NiMo-TiC coatings. XRD, X-ray diffraction.

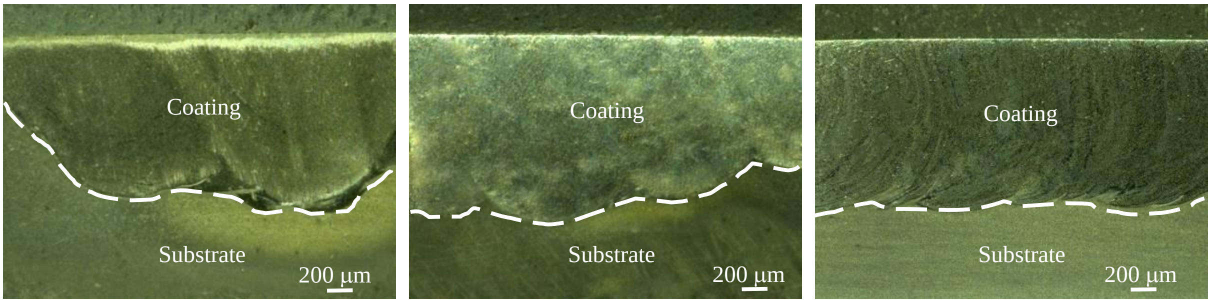

(a) (b) (c)

Fig. 5. Microstructure of the NiMo-TiC coating cross sections with different TiC mass fractions: **(a)** NiMo-5%TiC coating; **(b)** NiMo-15%TiC coating; **(c)** NiMo-25%TiC coating.

sult, the porosity was related to the wear resistance, and the porosity decreased with the TiC mass fraction, which was conducive to improving the wear resistance of the NiMo-TiC coating.

3.2. XRD patterns of powder and coating surfaces

Figure 4(a) shows the XRD patterns of the NiMo-5%TiC, NiMo-15%TiC, and NiMo-25%TiC powders. The mixed powder was composed of NiMo and TiC phases, where the peak intensity of TiC increased with the TiC mass fraction, while that of NiMo correspondingly decreased. Figure 4(b) shows the XRD patterns of NiMo-5%TiC, NiMo-15%TiC, and NiMo-25%TiC coatings. It could be seen that the C in the powder generated the carbides Ni_3C and Fe_2C at high temperatures, which had high hardness [23, 24]. Meanwhile, the Mo balanced the Ni_3Mo to form NiMo and Mo_2C through chemical reactions.

3.3. Microstructure of coating cross sections

The microstructures of the NiMo-5%TiC, NiMo-15%TiC, and NiMo-25%TiC coating cross-sections are shown in Figure 5. There was no gap between the coatings and the substrate, which indicated that the coatings were tightly bonded with the substrate. In addition, the wavy profiles were found at the coating-substrate interfaces because the laser energy density had a Gaussian distribution and the energy at the center is higher than that at the edge [25]. It was concluded that the composition of NiMo-TiC had little effect on the bonding between the coatings and the substrate.

3.4. Hardness distributions

Figure 6(a) shows the hardness of the substrate and the NiMo-TiC coating surfaces. The average hardness of the substrate, NiMo-5%TiC, NiMo-15%TiC, and NiMo-25%TiC coatings was $540HV_{0.5}$, $872HV_{0.5}$, $936HV_{0.5}$, and $1{,}015HV_{0.5}$ respectively, showing that the coating hardness was significantly higher than that of the substrate. The coating hardness increased with the increase of TiC mass fraction because the TiC had the effect of grain refinement, as shown in Figure 2, which can strengthen the coating hardness [26, 27].

Figure 6(b) shows the hardness distributions of NiMo-5%TiC, NiMo-15%TiC, and NiMo-25%TiC coating cross-sections. The hardness of coating, diffusion layer, heat-affected layer, and substrate presented a downward trend. Among them, the diffusion layer was a metallurgical bonding zone formed by fusing the melting liquid phase of the substrate and the coating, and its hardness was between that of the coating and the substrate [28].

3.5. COF analysis

COF was an important index to evaluate the friction-wear performance of the coatings. Figure 7 shows the curves of COFs versus the wear time of the substrate and the NiMo-TiC coatings, and the wear process was divided into running-in and stable wear periods [29, 30]. The average COFs of the substrate and the NiMo-5%TiC,

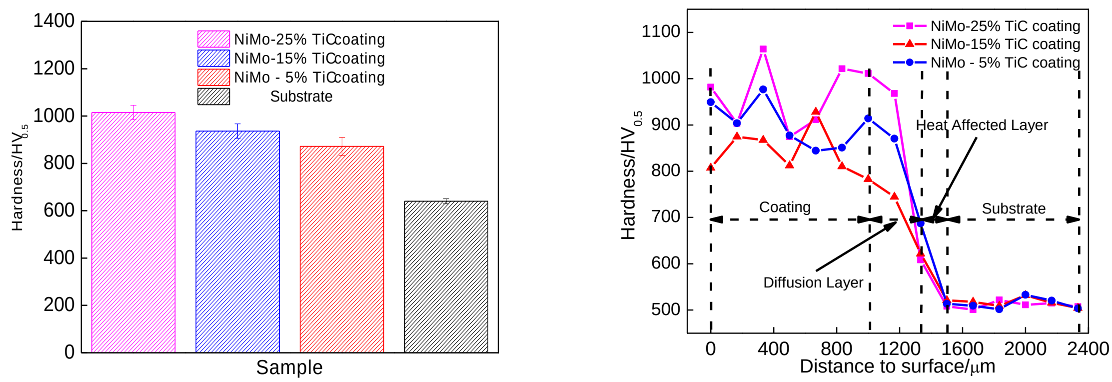

(a) (b)

Fig. 6. Hardness of NiMo-TiC coating surfaces and cross sections with different TiC mass fractions: **(a)** surface hardness; **(b)** cross section hardness.

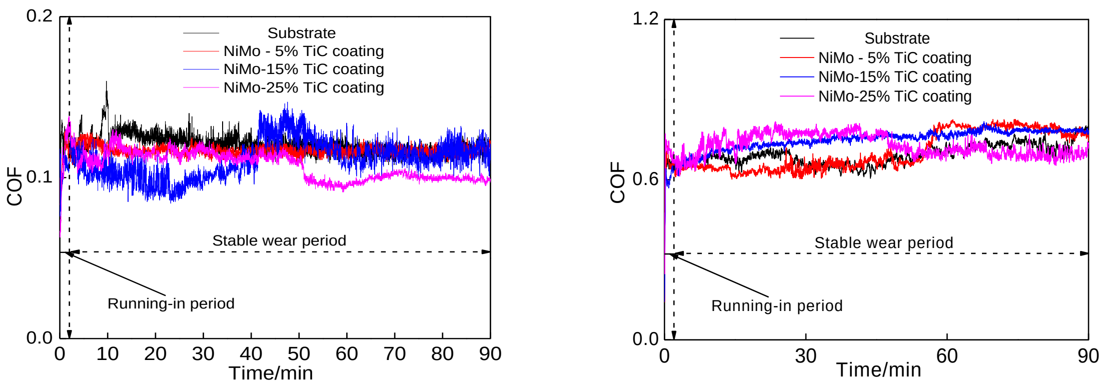

(a) (b)

Fig. 7. COFs versus wear time of the substrate and the NiMo-TiC coatings with different TiC mass fractions under grease-lubrication and dry-friction conditions: **(a)** under grease-lubrication condition; **(b)** under dry-friction condition.

NiMo-15%TiC, and NiMo-25%TiC coatings under the grease-lubrication condition were 0.12, 0.116, 0.112, and 0.107, respectively, as shown in Figure 7(a). The average COFs of the substrate and the NiMo-5%TiC, NiMo-15%TiC, and NiMo-25%TiC coatings under the dry-friction condition were 0.747, 0.727, 0.703, and 0.692, respectively, as shown in Figure 7(b). The grease in the friction process formed a layer of lubricating film between the coating and the tribo-pair [31], and the COFs under the grease-lubrication condition were lower than those under the dry-friction condition, which indicated that the lubricating film played a role in friction reduction.

3.6. Profiles, wear rates, and widths of worn tracks

Figure 8(a) shows the profiles of worn tracks on the substrate and the NiMo-TiC coatings. The depths of worn tracks on the substrate, NiMo-5%TiC, NiMo-15%TiC, and NiMo-25%TiC coatings were 4.183 μm, 2.164 μm, 1.882 μm, and 1.246 μm, respectively, and the corresponding wear rates from Eq. (1) were 72.25 $\mu m^3/s/N$, 32.00 $\mu m^3/s/N$, 18.10 $\mu m^3/s/N$, and 7.99 $\mu m^3/s/N$, respectively, as shown in Figure 8(b). When the NiMo-TiC coatings came in contact with the hard tribo-pair surface, the TiC particles were exposed on the worn tracks, which transferred a high percentage of the normal load. This automatically re-

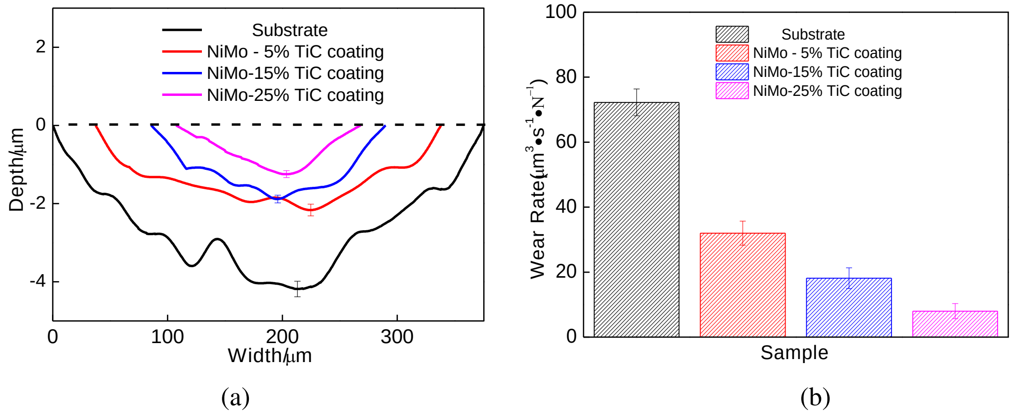

Fig. 8. Profiles of worn tracks and the wear rates of substrate and NiMo-TiC coatings with different TiC mass fractions under grease-lubrication condition: **(a)** profiles of worn tracks; **(b)** wear rates.

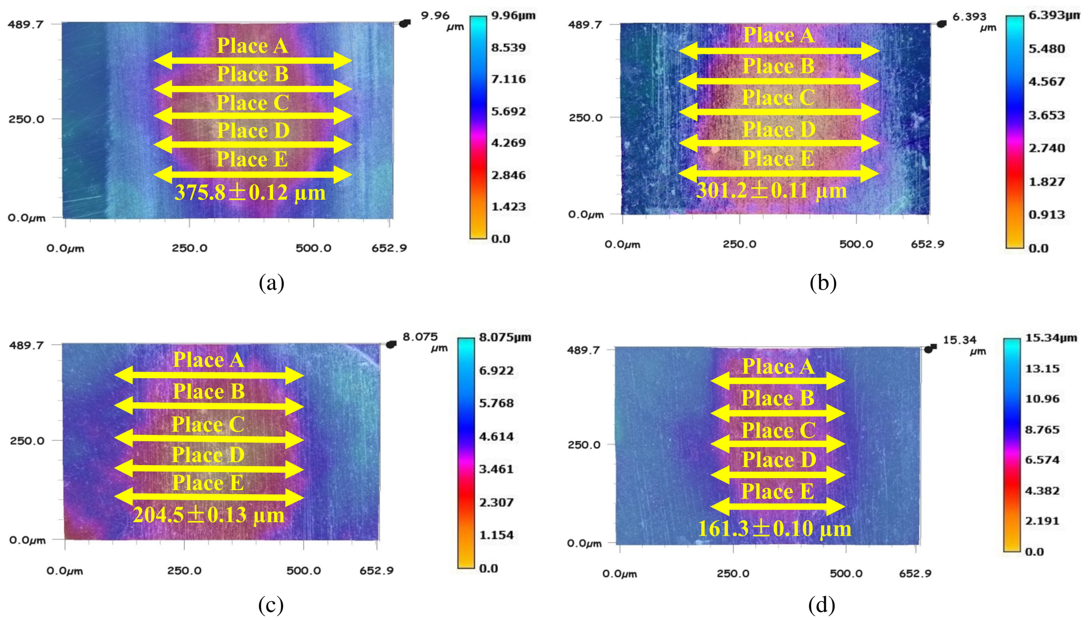

Fig. 9. Widths of the worn tracks on the substrate and on NiMo-TiC coating with different TiC mass fractions: **(a)** on substrate; **(b)** on NiMo-5%TiC coating; **(c)** on NiMo-15%TiC coating; **(d)** on NiMo-25%TiC coating.

duced the normal load on the worn track. Therefore, the TiC hard phase can reduce the wear rate of NiMo-TiC coatings [32].

The widths of the worn tracks on the substrate and on the NiMo-5%TiC, NiMo-15%TiC, and NiMo-25%TiC coatings are shown in Figure 9(a-d), in which the widths of the worn tracks were the average values of five observations. It indicated that the depths and widths of the worn tracks on the NiMo-TiC coatings were significantly shallower and narrower than those on the substrate. The wear resistance of the NiMo coatings was improved with the increase of TiC mass fraction, and the anti-wear performance of the NiMo-25%TiC coating was the highest among the three kinds of coatings.

The widths of the worn tracks on the tribo-pairs against the substrate and the NiMo-5%TiC, NiMo-15%TiC, and NiMo-25%TiC coatings are shown in Figure 10(a-d). It could be seen that the worn

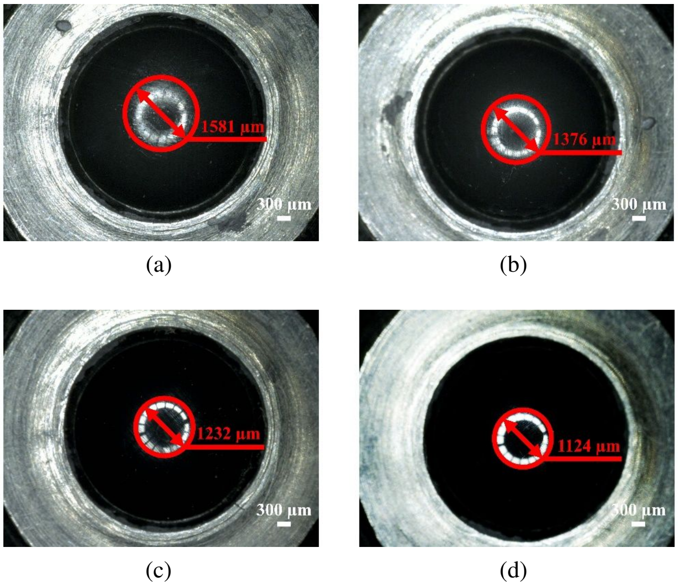

Fig. 10. Images of the worn tracks on tribo-pairs against the substrate and the NiMo-TiC coatings with different TiC mass fractions: **(a)** against substrate; **(b)** against NiMo-5%TiC coating; **(c)** against NiMo-15%TiC coating; **(d)** against NiMo-25%TiC coating.

square on the tribo-pairs decreased with the increase of TiC mass fraction. The worn tracks in Figure 10(a) was the most significant, and the worn tracks in Figure 10(b) was slightly better than that in Figure 10(a). Worn tracks were not observed in Figure 10(c) and 10(d) due to the shallow traces.

3.7. Morphologies of worn tracks

Figure 11(a) shows the morphology of the worn tracks on the substrate. From the low-magnification image, the profile of the worn tracks was obvious, while in the high-magnification image, there were obvious furrows on the worn track [30, 33]. As a result, the wear mechanism was concluded to be abrasive wear [34].

Figure 11(b) shows the morphology of the worn tracks on the NiMo-5%TiC coating. Its morphology under low magnification was vague; under high magnification, there were apparent furrows and small TiC particles. Compared with the substrate, the furrows on the worn track became shallower and thinner, and the wear mechanism was also abrasive wear.

Figure 11(c) shows the morphology of worn tracks on the the NiMo-15%TiC coating. Under low magnification, the morphology of the worn tracks was indistinct; under high magnification, the number of furrows further decreased compared with the worn tracks on the substrate and the NiMo-5%TiC coating, and the TiC particles became bigger and more visible on the worn tracks. It was concluded that the wear resistance was higher than in the NiMo-5%TiC coating, and the main wear mechanism was abrasive wear.

Figure 11(d) shows the morphology of the worn tracks on the NiMo-25% coating. The morphology of the worn tracks under low and high magnifications were similar to those of the NiMo-15%TiC coating, and the wear mechanism of the coating was also abrasive wear.

3.8. Line scan analysis of worn tracks

Figure 12(a) shows the line scan analysis of the worn track on the substrate, whereby the Fe, C, and Cr were detected on the worn track. The C and Cr were distributed evenly on the worn tracks, indicating that C and Cr were the anti-wear elements, while Fe was worn away in the friction process [35].

Figure 12(b) shows the line scan analysis of

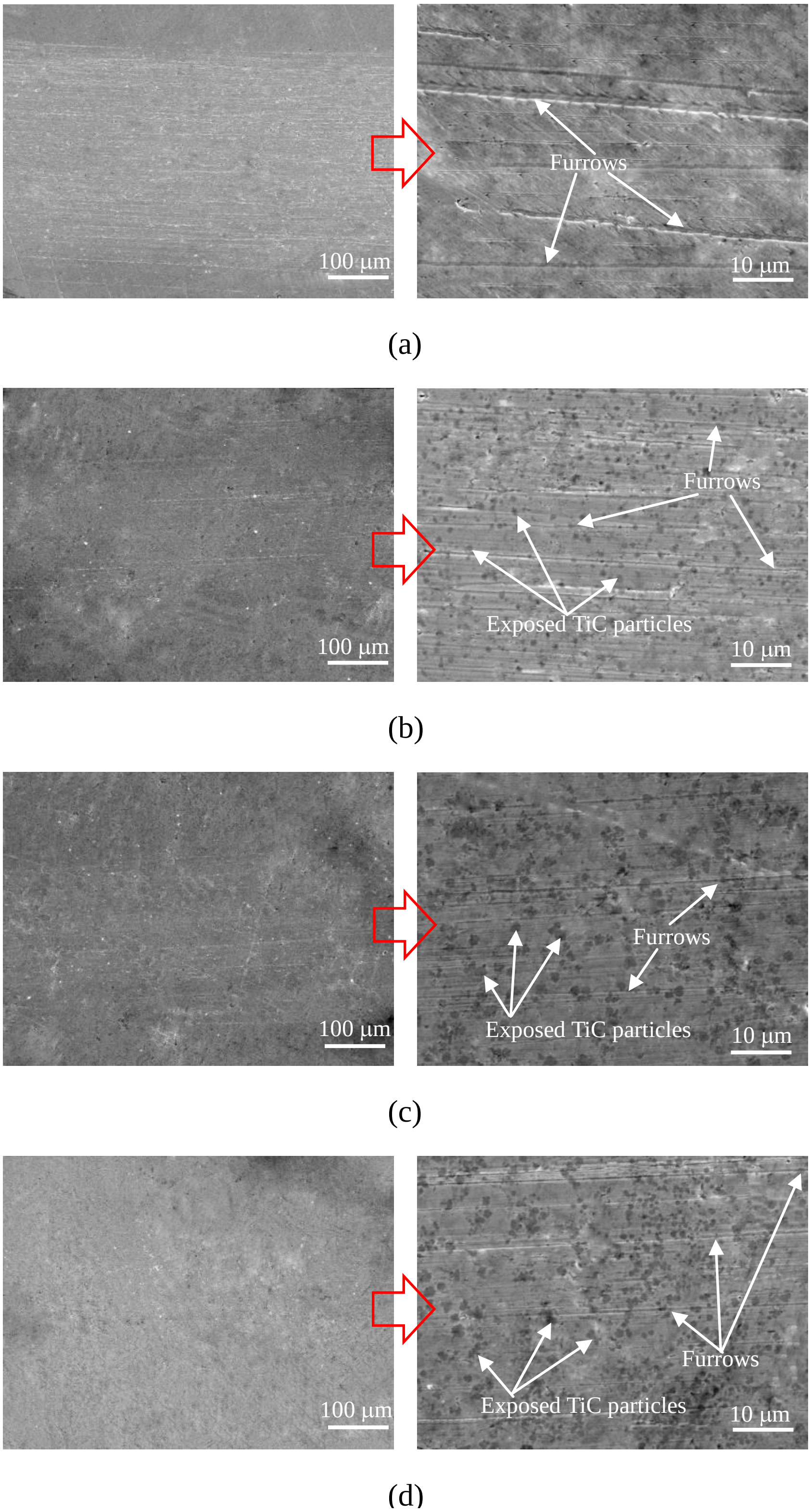

Fig. 11. Morphologies of the worn tracks on the substrate and on the NiMo-TiC coatings with different TiC mass fractions: **(a)** substrate; **(b)** NiMo-5%TiC coating; **(c)** NiMo-15%TiC coating; **(d)** NiMo-25%TiC coating.

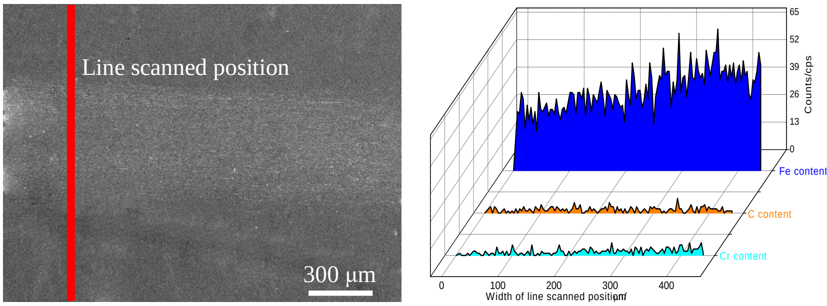

(a)

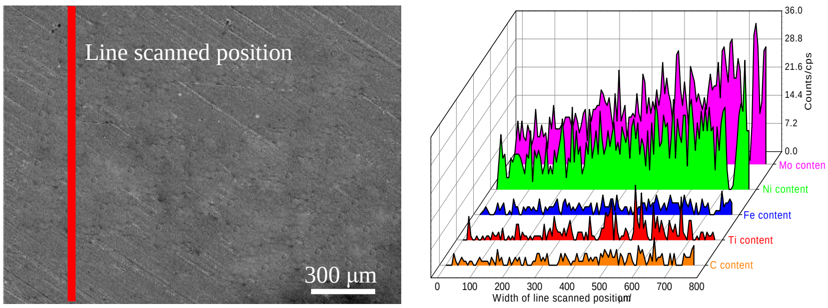

(b)

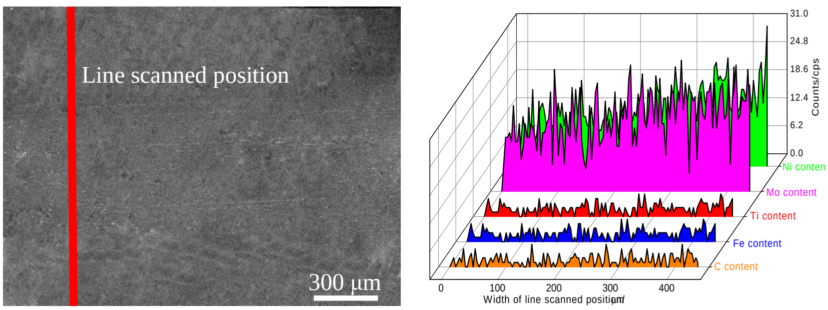

(c)

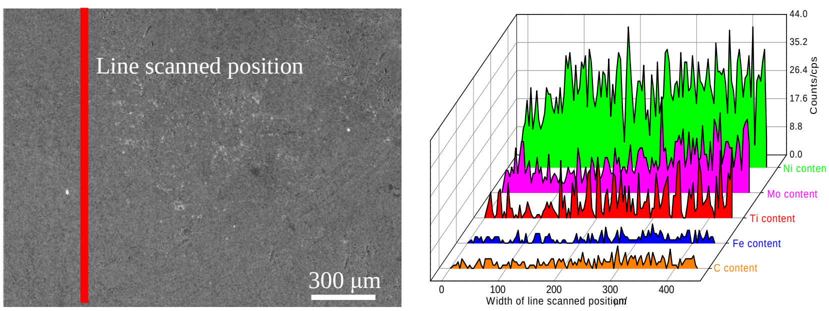

(d)

Fig. 12. EDS line scan analysis of the worn tracks on NiMo-TiC coating with different TiC mass fractions: **(a)** on substrate; **(b)** on NiMo-5%TiC coating; **(c)** on NiMo-15%TiC coating; **(d)** on NiMo-25%TiC coating.

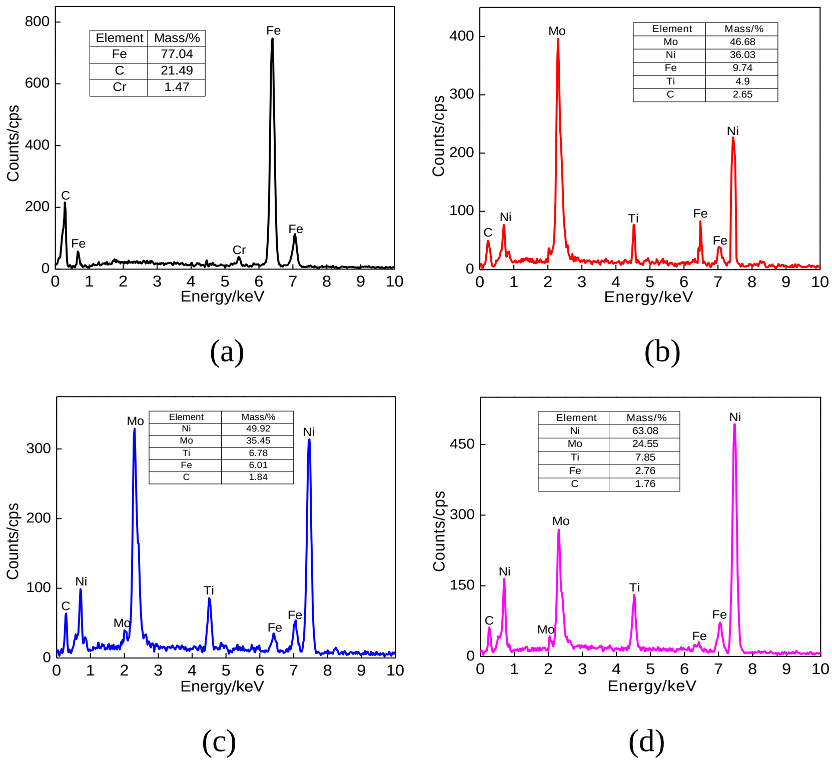

Fig. 13. EDS analysis of the worn tracks on the substrate and the NiMo-TiC coatings with different TiC mass fractions: **(a)** substrate; **(b)** NiMo-5%TiC coating; **(c)** NiMo-15%TiC coating; **(d)** NiMo-25%TiC coating.

the worn track on the NiMo-5%TiC coating. The Mo, Ni, Fe, Ti, and C were detected on the worn track, in which the Fe originated from the diluted elements of the substrate. The counts of Mo, Ni, and Fe on the worn track were lower than those on the unworn coating, which were worn away in the friction process. However, the Ti and C were lost slightly, which played a role in the wear resistance.

Figure 12(c) shows the line scan analysis of the worn track on NiMo-15%TiC coating. Ni, Mo, Ti, Fe, and C were also detected on the worn track, and the Fe came from the substrate due to the dilution effect. The counts of Ni and Fe on the tracks declined, and the loss in counts of Ni was the most for the composition among the three kinds of coating. It also could be seen that Mo also acted as a lubricant, and the Ti and C exerted wear resistance.

Figure 12(d) shows the line scan analysis of the worn track on NiMo-25%TiC coating. Ni, Mo, Ti, Fe, and C were detected on the worn track, in which the Fe was derived from the substrate due to the dilution effect. It could be seen that Ni, Mo, and Fe were the main phases, which were worn away in the friction process, while Ti and C were reserved due to their high hardness.

From the above analysis, it was concluded that the contents of the Ti and C on the worn tracks increased with the mass fraction of TiC, and the wear resistance of NiMo-TiC coatings was improved due to the presence of the TiC with high hardness.

The result of the EDS analysis of the worn track on the substrate in Figure 12(a) is shown in Figure 13(a). The mass fractions of Fe, C, and Cr were 77.04%, 21.49%, and 1.47%, respectively. Figure 13(b-d) shows the EDS analysis results of the worn tracks on the NiMo-5%TiC, NiMo-15%TiC, and NiMo-25%TiC coatings. The mass fractions of Ni and Mo decreased with increase of TiC mass fraction, and the mass fractions of Ti showed the upward trend, indicating that TiC improved the anti-wear performance of NiMo-TiC coatings [36].

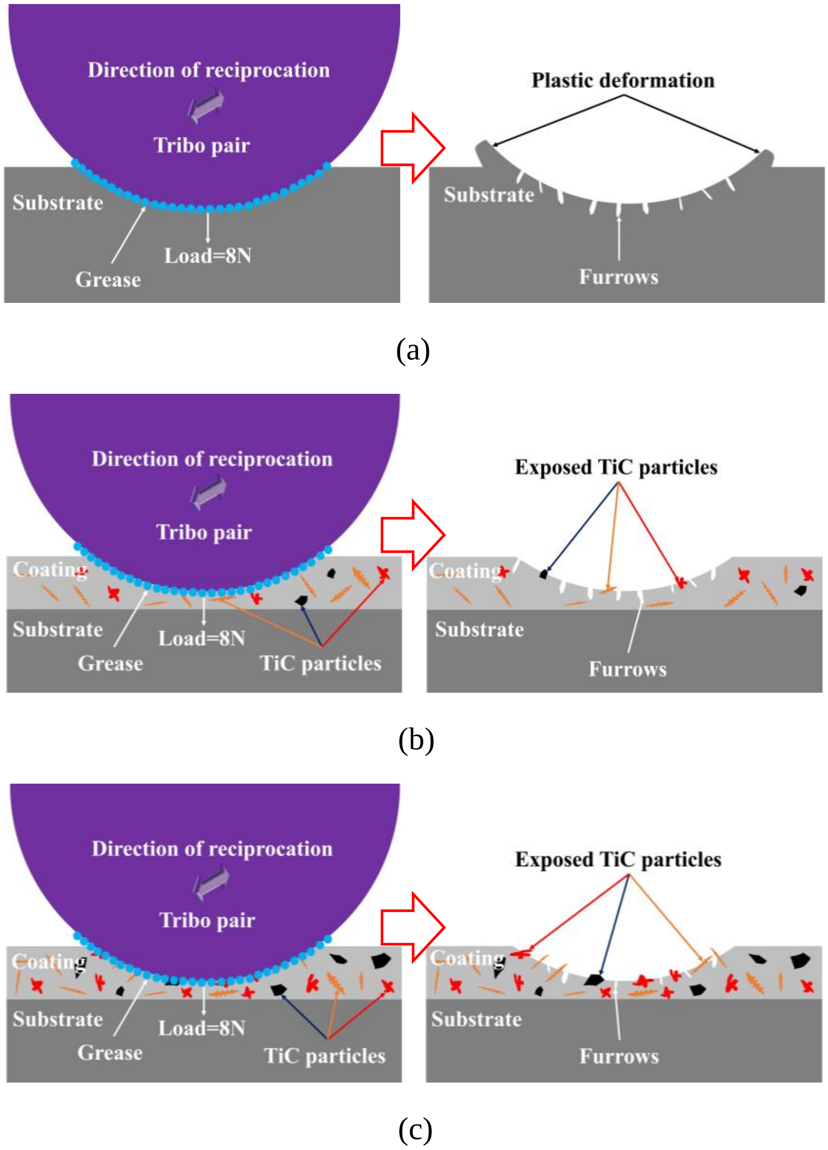

Fig. 14. Wear models of substrate and NiMo-TiC coatings with different TiC mass fractions: **(a)** substrate; **(b)** NiMo-5%TiC coating; **(c)** NiMo-15%TiC and NiMo-25%TiC coatings.

3.9. Wear mechanisms

Under the action of normal load, the substrate easily produced plastic deformation due to its low hardness. The Fe in Figure 12(a) was worn away by the tribo-pair, and the furrows in Figure 11(a) occurred on the worn track. The furrows came from the micro-cutting by the tribo-pair, as shown in Figure 14(a). Therefore, the wear mechanism was abrasive wear [36].

The NiMo-TiC coatings underwent a series of complex chemical reactions to form the hard carbides of Ni_3C and Fe_2C in Figure 4(b), which enhanced the coating hardness [34]. The worn tracks were prone to formation of furrows, as shown in Figure 11(b), which were plowed by the tribo-pair. And the tribo-pair produced micro-cutting which revealed that the wear mechanism of the NiMo-5%TiC coating was abrasive wear too, as shown in Figure 14(b). From Figure 12(b), it could be seen that the Mo, Ni, and Fe were worn away in the friction process, and the TiC did not exert the anti-wear performance due to its low mass friction. In this case, the furrows on the worn track were less and thinner than those on the substrate.

There were furrows on the worn tracks of the NiMo-15%TiC and NiMo-25%TiC coatings in Figure 11(c) and 11(d), as shown in Figure 14(c). The furrows were plowed by the tribo-pair, which produced micro-cutting. And it indicated that the wear mechanism was abrasive wear. From Figure 12(c) and 12(d), it could be seen that the Ni and Fe participated in the friction process and were worn away. With the continuation of the test over a longer period, the reinforced phase of TiC was gradually exposed on the worn tracks in Figure 11(c) and 11(d), indicating that its anti-wear capability was better than those of Ni and Mo [18]. It was concluded that the anti-wear performance of NiMo-TiC coatings enhanced with the increase of TiC mass fraction, and the wear resistance of NiMo-25%TiC coating was the best among the three kinds of coatings.

4. Conclusions

1. The surface hardness of NiMo-5%TiC, NiMo-15%TiC, and NiMo-25%TiC coatings increases from 872$HV_{0.5}$ to 1,015$HV_{0.5}$ with the increase of TiC mass fraction, which is because the TiC has the effect of grain refinement, and this effect can strengthen the coating hardness. Moreover, the hardness of TiC-reinforced NiMo coatings increases with the decrease of coating porosity.
2. The average COFs of NiMo-5%TiC, NiMo-15%TiC, and NiMo-25%TiC coatings under the grease-lubrication condition are 0.116, 0.112, and 0.107, respectively, and the corresponding wear rates are 32.0 $\mu m^3/s/N$, 18.10 $\mu m^3/s/N$, and 7.99 $\mu m^3/s/N$, respectively, which indicates that the NiMo-25%TiC coating has the best wear resistance.
3. The wear mechanism of the NiMo-TiC coatings is abrasive wear, which is contributed to the friction reduction role of the TiC phase with high hardness. TiC addition improves the wear resistance of TiC-reinforced NiMo coatings in the friction process, and their anti-wear performance is enhanced with increase of the TiC mass fraction.

References

[1] Zhao Y, Cui C, Han X, Cui S, Li N, Qian Z. Preparation of in situ NbC-TiC@Graphene/Fe composite inoculant and its effect on microstructures and properties of GCr15. Mat Sci Eng A-Struct. 2020;772:138737; https://doi.org/10.1016/j.msea.2019.138737

[2] El Laithy M, Wang L, Harvey TJ, Vierneusel B, Correns M, Blass T. Further understanding of rolling contact fatigue in rolling element bearings -A review. Tribol Int. 2020;140:138737; https://doi.org/10.1016/j.triboint.2019.105849

[3] Cerrada M, Sánchez RV, Li C, Pacheco F, Cabrera D, de Oliveirae JV, et al. A review on data-driven fault severity assessment in rolling bearings. Mech Syst Signal Pr. 2018;99:169-96; https://doi.org/10.1016/j.ymssp.2017.06.012

[4] Zikin A, Badisch E, Hussaionva I, Tomastik C, Danninger H. Characterization of TiC-NiMo reinforced Ni-based hardfacing. Surf Coat Technol. 2013;236:36-44; https://doi.org/10.1016/j.surfcoat.2013.02.027

[5] Tan YF, Long HE, Wang XL, Hong X, Wang WG. Tribological properties and wear prediction model of TiC particles reinforced Ni-base alloy composite coatings. Trans Nonferr Metal Soc. 2014;24:2566-73; https://doi.org/10.1016/S1003-6326(14)63384-7

[6] Téllez-Villaseñor MA, León-Patiño CA, Aguilar-Reyes EA, Bedolla-Jacuinde A. Effect of load and sliding velocity on the wear behaviour of infiltrated TiC/Cu-Ni composites. Wear. 2021;484-485:203667; https://doi.org/10.1016/j.wear.2021.203667

[7] Wang R, Zhu GL, Yang C, Zhou WZ, Wang DH, Dong AP, et al. Novel selective laser melting processed in-situ TiC particle-reinforced Ni matrix composite with excellent processability and mechanical properties. Mat Sci Eng A-Struct. 2020;797:140145; https://doi.org/10.1016/j.msea.2020.140145

[8] Kübarsepp J, Klaasen H, Pirso J. Behaviour of TiC-base cermets in different wear conditions. Wear. 2001;249:229-34; https://doi.org/10.1016/S0043-1648(01)00569-5

[9] Hussainova I. Effect of microstructure on the erosive wear of titanium carbide-based cermets. Wear. 2003;255:121-8; https://doi.org/10.1016/S0043-1648(03)00198-4

[10] Zhu LD, Xue PS, Lan Q, Meng GR, Ren Y, Yang ZC, et al. Recent research and development status of laser cladding: A review. Opt Laser Tech-

nol. 2021;138:106915; https://doi.org/10.1016/j.optlastec.2021.106915
[11] Majumdar JD, Galun R, Mordike BL, Manna I. Effect of laser surface melting on corrosion and wear resistance of a commercial magnesium alloy. Mat Sci Eng A-Struct. 2003;361(1-2):119-29; https://doi.org/10.1016/S0921-5093(03)00519-7
[12] Nurminena J, Näkki J, Vuoristo P. Microstructure and properties of hard and wear resistant MMC coatings deposited by laser cladding. Int J Refract Met H. 2009;27(2):472-8; https://doi.org/10.1016/j.ijrmhm.2008.10.008
[13] Huang L, Deng XT, Wang Q, Jia Y, Li CR, Wang ZD. Solidification and sliding wear behavior of low-alloy abrasion-resistant steel reinforced with TiC particles. Wear. 2020;458-459:203444; https://doi.org/10.1016/j.wear.2020.203444
[14] Lin CL, Meehan PA. Morphological and elemental analysis of wear debris naturally formed in grease lubricated railway axle bearings. Wear. 2021;484-485:203994; https://doi.org/10.1016/j.wear.2021.203994
[15] Lu JZ, Cao J, Lu HF, Zhang LY, Luo KY. Wear properties and microstructural analyses of Fe-based coatings with various WC contents on H13 die steel by laser cladding. Surf Coat Technol. 2019;369:228-37; https://doi.org/10.1016/j.surfcoat.2019.04.063
[16] Zhou J, Kong D. Microstructure, Tribological performance, and wear mechanism of Cr- and Mo-reinforced FeSiB coatings by laser cladding. J Mater Eng Perform. 2020;29:7428-44; https://doi.org/10.1007/s11665-020-05187-w
[17] Zhang PL, Li MC, Yan H, Chen JS, Yu ZS, Ye X. Microstructure evolution of Ni-Mo-Fe-Si quaternary metal silicide alloy composite coatings by laser cladding on pure Ni. J Alloy Compd. 2019;785:984-1000; https://doi.org/10.1016/j.jallcom.2019.01.191
[18] Jiang PF, Zhang CH, Zhang S, Zhang JB, Chen J, Liu Y. Fabrication and wear behavior of TiC reinforced FeCoCrAlCu-based high entropy alloy coatings by laser surface alloying. Mater Chem Phys. 2020;255:123571; https://doi.org/10.1016/j.matchemphys.2020.123571
[19] Dadoo A, Boutorabia SMA. Correlation between pulsed laser parameters and MC carbide morphology in H13 tool steel/TiC composite coating. Opt Laser Technol. 2020;127:106120; https://doi.org/10.1016/j.optlastec.2020.106120
[20] Chen H, Lu YY, Sun YS, Wei YF, Wang XY, Liu DJ. Coarse TiC particles reinforced H13 steel matrix composites produced by laser cladding. Surf Coat Technol. 2020;395:125867; https://doi.org/10.1016/j.surfcoat.2020.125867
[21] Han TF, Xiao M, Zhang Y, Shen YF. Effects of graphite and graphene spatial structure on the TiC crystal structure and the properties of composite coatings. Surf Coat Technol. 2019;377:124909; https://doi.org/10.1016/j.surfcoat.2019.124909
[22] Tejero-Martin D, Bai MW, Mata J, Hussain T. Evolution of porosity in suspension thermal sprayed YSZ thermal barrier coatings through neutron scattering and image analysis techniques. J Eur Ceram Soc. 2021;41(12):6035-48; https://doi.org/10.1016/j.jeurceramsoc.2021.04.020
[23] Liu WH, Zeng W, Liu FS, Tang B, Liu QJ, Wang WD. The mechanical and electronic properties of o-Fe2C, h-Fe3C, t-Fe5C2, m-Fe5C2 and h-Fe7C3 compounds: First-principles calculations. Phys B. 2021;606:412825; https://doi.org/10.1016/j.physb.2021.412825
[24] Braic M, Balaceanu M, Parau AC, Dine M, Vladescu A. Investigation of multilayered TiSiC/NiC protective coatings. Vacuum. 2015;120(A):60-6; https://doi.org/10.1016/j.vacuum.2015.06.019
[25] Zhou JL, Kong DJ. Immersion corrosion and electrochemical performances of laser cladded FeSiB, FeSiBCr and FeSiBCrMo coatings in 3.5 wt% NaCl solution. Surf Coat Technol. 2020;383:125229; https://doi.org/10.1016/j.surfcoat.2019.125229
[26] Liu H, Liu J, Chen PJ, Yang HF. Microstructure and high temperature wear behaviour of in-situ TiC reinforced AlCoCrFeNi-based high-entropy alloy composite coatings fabricated by laser cladding. Opt Laser Technol. 2019;118:140-50; https://doi.org/10.1016/j.optlastec.2019.05.006
[27] Zhu HM, Ouyang MN, Hu JP, Zhang JW, Qiu CJ. Design and development of TiC-reinforced 410 martensitic stainless steel coatings fabricated by laser cladding. Ceram Int. 2021;47:12505-13; https://doi.org/10.1016/j.ceramint.2021.01.108
[28] Cui G, Han B, Zhao JB, Li MY. Comparative study on tribological properties of the sulfurizing layers on Fe, Ni and Co based laser cladding coatings. Tribol Int. 2019;134:36-49; https://doi.org/10.1016/j.triboint.2019.01.019
[29] Muhaffel F, Kaba M, Cempura G, Derin B, Kruk A, Atar E, et al. Influence of alumina and zirconia incorporations on the structure and wear resistance of titania-based MAO coatings. Surf Coat Technol. 2019;377:124900; https://doi.org/10.1016/j.surfcoat.2019.124900
[30] Zhang Q, Wu ZT, Xu YX, Wang QM, Chen L, Kim KH. Improving the mechanical and anti-wear properties of AlTiN coatings by the hybrid arc and sputtering deposition. Surf Coat Technol. 2019;378:125022; https://doi.org/10.1016/j.surfcoat.2019.125022
[31] Larsson E, Westbroek R, Leckner J, Jacobson S, Rudolphi ÅK. Grease-lubricated tribological contacts-Influence of graphite, graphene oxide and reduced graphene oxide as lubricating additives in lithium complex (LiX)- and polypropylene (PP)-thickened greases. Wear. 2021;486-487:204107; https://doi.org/10.1016/j.wear.2021.204107
[32] León-Patiño CA, Braulio-Sánchez M, Aguilar-Reyes EA, Bedolla-Becerril E, Bedolla-Jacuinde A. Dry

sliding wear behavior of infiltrated particulate reinforced Ni/TiC composites. Wear. 2019;426-427:989-95; https://doi.org/10.1016/j.wear.2019.01.074
[33] Zhou JL, Kong DJ. Effects of Al and Ti additions on corrosive-wear and electrochemical behaviors of laser cladded FeSiB coatings. Opt Laser Technol. 2019;124:105958; https://doi.org/10.1016/j.optlastec.2019.105958
[34] Liu JS, Shi Y. Microstructure and wear behavior of laser-cladded Ni-based coatings decorated by graphite particles. Surf Coat Technol. 2021;412:127044; https://doi.org/10.1016/j.surfcoat.2021.127044
[35] Shi JZ, Ge Y, Kong DJ. Microstructure, dry sliding friction performances and wear mechanism of laser cladded WC-10Co4Cr coating with different Al_2O_3 mass fractions. Surf Coat Technol. 2021;406:126749; https://doi.org/10.1016/j.surfcoat.2020.126749
[36] Cai YC, Zhu LS, Cui Y, Shan MD, Li HJ, Xin Y, et al. Fracture and wear mechanisms of FeMnCrNiCo + x(TiC) composite high-entropy alloy cladding layers. Appl Surf Sci. 2021;543:148794; https://doi.org/10.1016/j.apsusc.2020.148794

Received 2021-06-04
Accepted 2021-11-17